01,05,07,15

Magnetic phase temperature-pressure diagram of FeRh alloy with $Fe_{94}Rh_6$ phase

© T.R. Arslanov, A.A. Amirov, L.N. Khanov

Amirkhanov Institute of Physics, Daghestan Federal Research Center, Russian Academy of Sciences, Makhachkala, Russia

E-mail: arslanovt@gmail.com

Received November 20, 2024
Revised November 25, 2024
Accepted November 26, 2024

The *T-P* magnetic phase diagram of the $Fe_{50}Rh_{50}$ alloy with the $Fe_{94}Rh_6$ iron-rich phase has been studied based on the resistivity measurements under hydrostatic pressure. The Neel temperature $T_N \approx 370$ K up to pressures of 2 GPa shows a regular displacement with a positive pressure coefficient of +42.3 K/GPa. The effect of the $Fe_{94}Rh_6$ phase on the T_N is revealed at high pressures ($P > 3.5$ GPa), at which the triple point region on the phase diagram is rounded due to the possible formation of a new high-pressure antiferromagnetic structure.

Keywords: FeRh, high pressure, B2 structure, resistivity, Neel temperature, magnetic phase diagram.

DOI: 10.61011/PSS.2024.12.60205.314

1. Introduction

Recently the interest in unique properties of intermetallic ferrum and rhodium (FeRh) compound is caused by the ability to produce thin-film forms on its basis, oriented at improvement of device architecture [1–6]. Parallel to this, volume forms of FeRh fill a special place in the hierarchy of magnetocaloric materials in connection with prevalence of substantial variations of entropy in the process of magnetic phase change of order I [7–9]. However, despite practical significance and multiple studies of recent years, the physical nature of phase change in FeRh, found more than half a century ago [10], still remains contradictory.

The ordered compound $Fe_{50}Rh_{50}$ may be implemented in two types of crystalline modifications: chemically ordered structure bcc-B2 (type CsCl) and disordered structure fcc at room temperature. Being in fcc phase, the alloy will not show noticeable magnetic properties [11]. Besides, bcc phase is antiferromagnetic of G-type and undergoes an isostructural magnetic phase transition of order I from antiferromagnetic phase to ferromagnetic phase in area ~ 370 K with temperature increase [10,12]. As temperature increases further, ferromagnetic phase changes to paramagnetic phase at $T_C = 670$ K [12]. „Low-temperature“ phase bcc-B2 is characterized by magnetic structure, where local Fe moments are $\pm 3\,\mu_B$, and nearly zero moments are placed on Rh atoms, whereas in the high-temperature ferromagnetic phase local moments of ferrum and rhodium are $\sim 3.2\,\mu_B$ and $\sim 1\,\mu_B$, respectively. Phase change between these two magnetic structures happens by metamagnetic transition, accompanied by volume expansion of cubic phase $\sim 1\%$ and high drop of resistivity, which indicates a close connection between electronic, magnetic and structural properties in an alloy [12,13].

Studies of FeRh magnetic properties within the estimates from first principles mostly converge on a position that the decisive role in the magnetic transformation mechanism is played by local moments of Rh [14,15]. A similar conclusion also follows from the studies under high pressure, which note that Rh atoms have no magnetic torque being in antiferromagnetic and paramagnetic phases of high pressure [16]. Besides, the transition temperature of the first order transition (T_N) under high pressure increases, stabilizing the antiferromagnetic state in a wide area *T-P* of the phasing diagram, and the transition temperature at T_C on the contrary demonstrates decrease. Besides, existence of a triple point is discussed on *T-P* magnetic phasing diagram, where antiferromagnetic, ferromagnetic and paramagnetic phases may coexist [16–19].

This paper considers the effect of the iron fortified phase $Fe_{94}Rh_6$ in the ordered alloy $Fe_{50}Rh_{50}$ at the state of its *T-P* magnetic phasing diagram. Within this study, high-temperature measurements of resistivity were made under pressure, mainly focused on the temperature of the transition from the antiferromagnetic state to the ferromagnetic state. It is shown that the presence of phase $Fe_{0.94}Rh_{0.06}$ causes bypass of the phase line of Neel temperature from the suggested triple point on *T-P* magnetic phasing diagram $Fe_{50}Rh_{50}$.

2. Experimental procedure

The specimen of $Fe_{50}Rh_{50}$ compound was produced by the method of arc welding from pure elements of rhodium Rh (99.9%) and ferrum (99.99%). After melting, the specimen was exposed to homogenizing annealing at temperature $T = 1000°C$ for a week, then it was cleaned and cut in the form of a plate. For subsequent characterization of the produced specimen by X-ray diffraction method, a fine

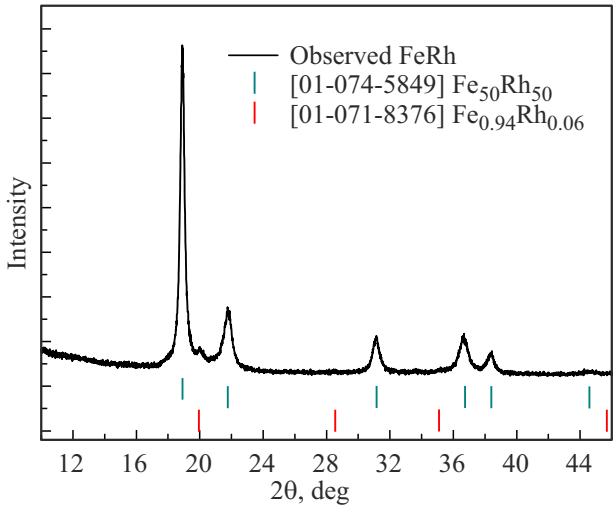

Figure 1. X-ray powder diffraction pattern of $Fe_{50}Rh_{50}$ specimen. The black line corresponds to experimental data, and the vertical little lines correspond to the position of Bragg peaks for phases $Fe_{50}Rh_{50}$ and $Fe_{0.94}Rh_{0.06}$, as specified in the legend.

fraction powder was used ($10-15\,\mu$m), which was received mechanically. Figure 1 shows a typical X-ray diffraction pattern of this powder. According to the data of X-ray phase analysis (XPA), a cubic phase of FeRh was identified in the specimen with spatial group Fm-$3m$ ($a = 3.74$ Å, $V = 52.31$ Å^3), the content of which was 95.4%. Apart from this primary phase, the XPA data noted the presence of 4.6% cubic phase $Fe_{0.94}Rh_{0.06}$ with spatial group Im-$3m$ ($a = 2.88$ Å, $V = 24.1$ Å^3).

The resistivity of the specimen was measured in the temperature range between 290 K and 470 K at high hydrostatic pressure in Toroid-15 chamber[20] using a modified six-pin method. The studied specimens were cut in the form of a parallelepiped with typical dimensions of $2.8 \times 0.9 \times 0.9$ mm^3. Direct current flowing through the sample was 100 mA. The pins to measure electric transport properties were made by soldering based on a tin-lead solder. The medium transmitting pressure in a fluoroplastic capsule with operating volume of 80 mm^3, polyethylsiloxane fluid (PES-5) was used, which enables high-temperature measurements under hydrostatic compression. The pressure inside the capsule was controlled using a manganin sensor calibrated by points of phase transitions in bismuth (2.55 GPa, 2.69 GPa, and 7.7 GPa).

3. Results and discussion

The natural feature of the temperature behavior of resistivity for most alloys of Fe-Rh system is the prevalence of the pronounced abnormality in the area of transformation from the antiferromagnetic phase to ferromagnetic phase, which is very similar to manifestation of the charge-density wave. Figure 2 shows the temperature dependence of the resistivity $\rho(T)$ for $Fe_{50}Rh_{50}$ specimen with the initial value of $\rho_0 = 2.32 \cdot 10^{-4}\,\Omega \cdot$ cm at atmospheric pressure. Under heating and subsequent cooling the dependence $\rho(T)$ demonstrates the specific hysteresis behavior in the region of the above phase transition of the first order and matches well with the data of previous research [12,13].

Temperature of magnetic transition in the heating mode defined as derivative $d\rho/dT$, is $T_N \approx 370$ K. From dependence $\rho(T)$ it should be noted that the presence of the additional phase $Fe_{94}Rh_6$ in the specimen at this stage demonstrates no contribution to the transport behavior.

Figure 3. shows the dependence of the resistivity on temperature $\rho(T, P)$ under high pressure values up to 3.47 GPa for $Fe_{50}Rh_{50}$ specimen, where the initial value is $\rho_0 = 1.98 \cdot 10^{-4}\,\Omega \cdot$ cm. As pressure rises, heating and cooling curves $\rho(T, P)$, and the regions of phase transformation move visibly towards the high temperatures. Already under pressure of $P = 3.45$ GPa Neel temperature

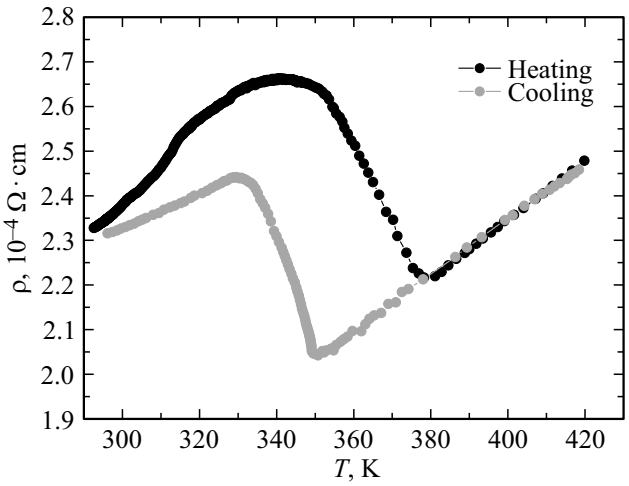

Figure 2. Temperature dependence of resistivity of $Fe_{50}Rh_{50}$ at atmospheric pressure, measured in the heating and cooling mode.

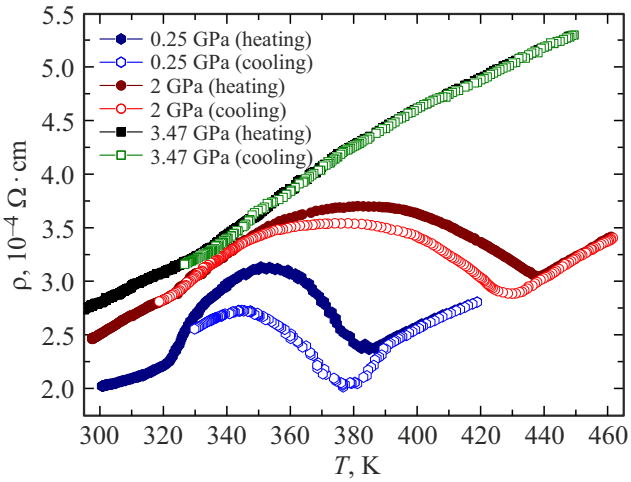

Figure 3. Temperature dependence of resistivity of $Fe_{50}Rh_{50}$ at various pressures up to 3.47 GPa, measured in the heating and cooling mode at atmospheric pressure.

goes beyond the limits of the measured temperature range ($T < 470$ K). The transition temperature T_N for pressures 0.25 GPa and 2 GPa was determined in a similar manner using minima of dependence $d\rho(T)/dT$ (see as example the insert to Figure 4) except for the curve under $P = 3.45$ GPa. The estimated value of baric coefficient in the range of these pressures is $dT_N/dP = +42.3$ K/GPa, which is very close to value +44 K/GPa from paper [17]. On the other hand, in accordance with the results of the same paper, the width of temperature hysteresis decreases as pressure increases, which indicates a gradual change in the order of the phase transformation from the first one to the second one. In this connection the absence of hysteresis for the curve $\rho(T, P)$ under 3.47 GPa in Figure 3 should not be associated with the occurrence of the phase transition of order II, since the magnetic phase transition has not yet been implemented.

It should be noted that such a strong displacement T_N with pressure rise to equiatomic $Fe_{50}Rh_{50}$ assumes that the baric coefficient dT_N/dP remains constant in sign up to pressures of $P = 8.3$ GPa. [17]. Our further measurements $\rho(T, P)$, made in the region of higher pressures ($P > 7$ GPa) found an unexpected behavior happening in our specimen. As shown in Figure 4, for pressures of $P = 7$ GPa and 7.7 GPa, the abnormal behavior $\rho(T, P)$, related probably to the same magnetic transformation from the antiferromagnetic state to the ferromagnetic one, is again implemented in the range of measured temperatures, which may mean the available trend of dT_N/dP sign change. As shown on the insert to Figure 4, dependence $d\rho(T)/dT$ notes values $T_N \approx 455$ K and $T_N \approx 450$ K for pressures $P = 7.15$ GPa and $P = 7.72$ GPa, accordingly. Therefore, reduction of T_N under $P > 7$ GPa, contradicts the results both for equiatomic compound $Fe_{50}Rh_{50}$, and for some nonstoichiometric and doped compounds $Fe_{49}Rh_{451}$, $Fe_{51.5}Rh_{48.5}$, $Fe_{50.5}Rh_{49.5}$, $Fe_{44}Rh_{49.5}Ir_{6.5}$ [17,21].

Another found feature of behavior $\rho(T, P)$ in Figure 4 is the presence of hysteresis, which demonstrates a minor jump in the region of $T = 320-322$ K with heating and more pronounced jump near $T = 334-336$ K in the cooling mode (Figure 4). According to data T-P the magnetic phasing diagram for $Fe_{50}Rh_{50}$ alloy above pressure of 6 GPa (in the region of the triple point) implements the phase transition of order II from the antiferromagnetic state to the paramagnetic one, when the when the ramp drops from dT_N/dP from +10 to +6 K/GPa [16,17], which it seems is not observed in our case.

The reasonable explanation for such behavior may be the fact of presence of phase $Fe_{94}Rh_6$, which start contributing to transport behavior at higher pressures.

Figure 5 provides comparison between the data $\rho(T, P)$, extracted from Figure 3 and Figure 4 at $T = 297$ K and baric dependence of direct measurements of $\rho(P)/\rho_0$ at the same temperature in specimen $Fe_{50}Rh_{50}$ with $\rho_0 = 2.345 \cdot 10^{-4}\ \Omega \cdot$ cm.

Both of these dependences, despite the difference in the source values ρ_0, demonstrate the maximum at $P \approx 3.45$ GPa. Note that such dome-like behavior $\rho(P)$ was observed for MnAs compound, which was accompanied with the magnetic transition induced by pressure, in particular, into the ferromagnetic phase of high pressure [22]. However, in case of $Fe_{50}Rh_{50}$ one may conclude that the change of baric motion $\rho(P)$ above 3.45 GPa is rather caused by effect of phase $Fe_{94}Rh_6$, which changes sign dT_N/dP.

Based on our data $\rho(T, P)$ to pressures of 7.72 GPa, an data of paper [17], T-P magnetic phasing diagram $Fe_{50}Rh_{50}$ was built (Figure 6). On this phasing diagram the value $T_N \sim 508$ K at $P = 3.45$ GPa was produced by extrapolation of data with account of constant baric coefficient $dT_N/dP = +42.3$ K/GPa up to this range of

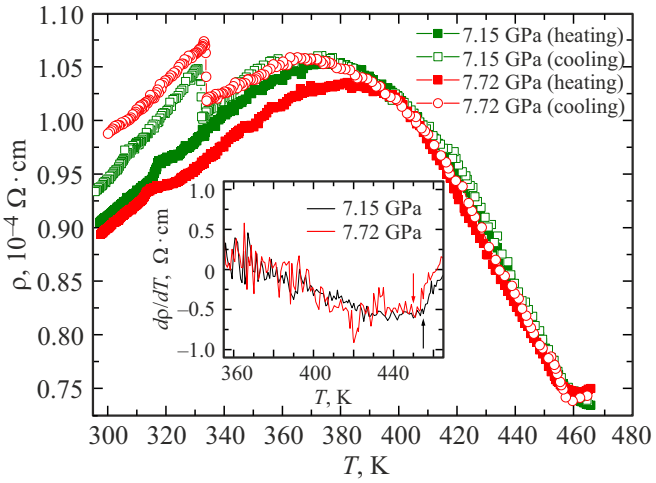

Figure 4. Temperature dependence of resistivity of $Fe_{50}Rh_{50}$ at pressures 7.15 GPa and 7.72 GPa, measured in the heating and cooling mode at atmospheric pressure. The insert contains temperature dependence $d\rho/dT$ for these pressures.

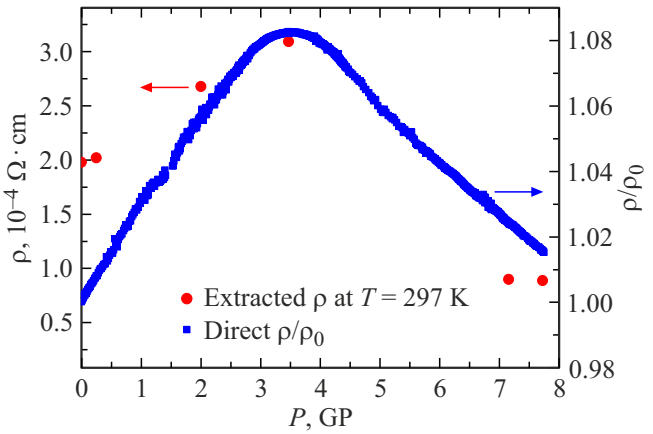

Figure 5. Dependences of resistivity for two samples $Fe_{50}Rh_{50}$ on pressure. The left scale along the axis of ordinates complies with values $\rho(T, P)$ extracted from Figure 3 and Figure 4 at $T = 297$ K, while the right scale displays the normalized value ρ/ρ_0 for specimen $Fe_{50}Rh_{50}$ with $\rho_0 = 2.345 \cdot 10^{-4}\ \Omega \cdot$ cm measured at isothermal increase of the pressure.

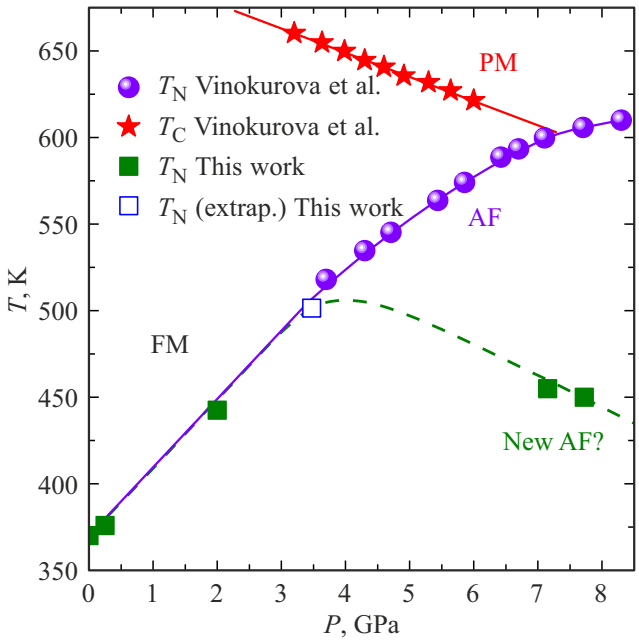

Figure 6. T-P magnetic phasing diagram $Fe_{50}Rh_{50}$, designed by changes of $\rho(T, P)$ and literature data [17]. Designations FM, AF, PM comply with ferromagnetic, antiferromagnetic and paramagnetic states, accordingly. Solid lines mean phase lines for temperatures T_N and T_C. The hatched line shows the bypass T_N from the region of the triple point, suggesting formation of a new AF phase.

pressures. As one may see, the qualitative behavior T_N for $Fe_{50}Rh_{50}$, containing phase $Fe_{94}Rh_6$, is visibly different, demonstrating the deviation of the phase line T_N of literature data. Reduction of T_N above pressure of 3.45 GPa may formally be treated as the absence of the triple point on the phasing diagram $Fe_{50}Rh_{50}$ due to bypass of the phase region where three phases coexist. In its turn it may indicate that the region of the high-temperature ferromagnetic phase will be stabilized with the pressure rise and tend towards the region of low temperatures.

The presence of the iron-enriched phase $Fe_{94}Rh_6$, even though insignificantly vs. the main cubic phase $Fe_{50}Rh_{50}$, but still may contribute strongly to magnetization of the specimen due to its ferromagnetic state. It is known that even insignificant deviation $(1-2\%)$ from the stoichiometric composition of the Fe-Rh system towards the increase of iron concentration may form a ferromagnetic order in the wide range of temperatures as it was shown for case $Fe_{51.5}Rh_{48.5}$ [21]. Therefore, our system $Fe_{50}Rh_{50}-Fe_{94}Rh_6$ will be characterized by the presence of such ferromagnetic contribution. Similarly to the conclusions in paper [21], one may conclude that gradual increase of resistivity together with pressure rise (Figure 5) is related to prevalence of ferromagnetic component for the specimen that is in inhomogeneous magnetic state (i.e. contains both ferro- and antiferromagnetic components). Under the conditions of high pressure, ferromagnetic phase $Fe_{94}Rh_6$ may be transformed into antiferromagnetic structure via the phase transition of order I, and this phase transformation matches the maximum point at $P \approx 3.5$ GPa (Figure 5). Further, as the resistivity reduces above 3.5 GPa, apart from the cubic antiferromagnetic structure $Fe_{50}Rh_{50}$, the antiferromagnetic structure $Fe_{94}Rh_6$ will be developed, which may result in formation of a new modulated antiferromagnetic structure different from the original one of G-type, as shown in T-P magnetic phasing diagram (Figure 6).

4. Conclusion

This study investigated the effect of phase $Fe_{94}Rh_6$, identified in equiatomic alloy $Fe_{50}Rh_{50}$, at the state of its T-P magnetic phasing diagram following the results of high-temperature studies of the resistivity up to pressures of 7.72 GPa. At atmospheric pressure the dependence $\rho(T)$ demonstrates phase transformation from the antiferromagnetic phase to the ferromagnetic phase at $T_N \approx 370$ K and displays no effect of phase $Fe_{94}Rh_6$. Displacement of T_N with application of pressure to 2 GPa happens with a ramp of $dT_N/dP = +42.3$ K/GPa, in good compliance with the literature data. The noticeable effect of phase $Fe_{94}Rh_6$ was found in the region of high pressures at $P > 7$ GPa, which results in reduction of T_N down to 450 K at $P = 7.72$ GPa. Deviation of the phase line T_N, happening above pressure of 3.45 GPa according to the data of dependence $\rho(P)$, indicates the absence of the triple point on T-P magnetic phasing diagram, and also the potential formation of a new antiferromagnetic high-pressure structure.

Funding

This study was supported financially by the Russian Science Foundation (RSF) under project No. 23-22-00324. The authors wish to thank A. Chirkova (Hochschule Bielefeld University of Applied Sciences and Arts, Bielefeld, Germany) for the provided specimen, valuable comments and discussions of the results.

Conflict of interest

The authors declare that they have no conflict of interest.

References

[1] D. Hamara, M. Strungaru, J. R. Massey, Q. Remy, X. Chen, G.N. Antonio, O.A. Santos, M. Hehn, R.F. L. Evans, R.W. Chantrell, S. Mangin, C. Ducati, C. H. Marrows, J. Barker, C. Ciccarelli, Nat. Commun. **15**, 4958 (2024).
[2] X. Yuan, Z. Zhang, R. Li, Q. Li, H. Lai, Y. Song, F. Liu, Y. Liu, Z. Lu, and R. Xiong. J. Alloys Compd. **1007**, 176330 (2024).
[3] K. Kang, H. Omura, D. Yesudas, O. Lee, K.-J. Lee, H.-W. Lee, T. Taniyama, G.-M. Choi. Nat. Commun. **14**, 3619 (2023).

[4] C. Cao, S. Chen, B. Cui, G. Yu, C. Jiang, Z. Yang, X. Qiu, T. Shang, Y. Xu, Q. Zhan. ACS Nano **16**, *8*, 12727–12737 (2022).
[5] D. G. Merkel, G. Hegedüs, M. Gracheva, A. Deák, L. Illés, A. Németh, F. Maccari, I. Radulov, M. Major, A.I. Chumakov, D. Bessas, D.L. Nagy, Z. Zolnai, S. Graning, K. Sájerman, E. Szilágyi. ACS Appl. Nano Mater. **5**, *4*, 5516–5526 (2022).
[6] D.G. Merkel, A. Lengyel, D.L. Nagy, A. Németh, Z.E. Horváth, C. Bogdán, M.A. Gracheva, G. Hegedüs, S. Sajti, G.Z. Radnóczi, E. Szilágyi. Sci. Rep. **10**, 13923 (2020).
[7] J.-Z. Hao, F.-X. Hu, Z.-B. Yu, F.-R. Shen, H.-B. Zhou, Y.-H. Gao, K.-M. Qiao, J. Li, C. Zhang, W.-H. Liang, J. Wang, J. He, J.-R. Sun, B.-G. Shen. Chin. Phys. B **29**, *4*, 047504 (2020).
[8] A.P. Kamantsev, A.A. Amirov, V.D. Zaporozhets, I.F. Gribanov, A.V. Golovchan, V.I. Valkov, O.O. Pavlukhina, V.V. Sokolovskiy, V.D. Buchelnikov, A.M. Aliev, V.V. Koledov. Metals **13**, *5*, 956 (2023).
[9] R. Joshi, S. Karmakar, K. Kumar, M. Gupta, R. Rawat. J. Appl. Phys. **133**, 173904 (2023).
[10] M. Fallot. Ann. Phys. **10**, 291 (1938).
[11] H. Miyajima, S. Yuasa. J. Magn. Magn. Mater. **202**, 104–107 (1992).
[12] J.S. Kouvel and C.C. Hartelius. J. Appl. Phys. **33**, 1343 (1962).
[13] L.H. Lewis, C.H. Marrows, S. Langridge. J. Phys. D: Appl. Phys. **49**, 323002 (2016).
[14] L.M. Sandratskii, P. Mavropoulos. Phys. Rev. B **83**, 174408 (2011).
[15] J.B. Staunton, R. Banerjee, M. dos S. Dias, A. Deak, L. Szunyogh. Phys. Rev. B **89**, 054427 (2014).
[16] R.C. Wayne. Phys. Rev. **170**, 523 (1968).
[17] L.I. Vinokurova, A.V. Vlasov, M. Pardavi-Horváth. Physica Status Solidi (b) **78**, *1*, 353–357 (1976).
[18] M.E. Gruner, P. Entel. Phase Transitions **78**, *1–3*, 209–217 (2005).
[19] E. Mendive-Tapia and T. Castán. Phys. Rev. B **91**, 224421 (2015).
[20] L.G. Khvostantsev, V.N. Slesarev, V.V. Brazhkin. High Pressure Res. **24**, 371 (2004).
[21] L.I. Vinokurova, A.V. Vlasov, N.I. Kulikov, M. Pardavi-Horváth. J. Magn. Magn. Mater. **25**, *2*, 201–206 (1981).
[22] T.R. Arslanov, L.N. Khanov, G.G. Ashurov, A.I. Ril. FTT **66**, *1*, 3–7 (2024).

Translated by M.Verenikina